Hydrodynamic Irreversibility in Creeping Flow

E. G. Flekkøy, T. Rage, U. Oxaal, and J. Feder
Department of Physics, University of Oslo, P.O. Box 1048 Blindern, 0316 Oslo 3, Norway
(Received 3 November 1995)

Using experiments as well as lattice Boltzmann and finite difference simulations we study creeping flow in a Hele-Shaw cell at Reynolds numbers below unity. We describe an "echo" technique that is very sensitive to effects of hydrodynamic irreversibility. By combining experimental and numerical studies we show that the irreversibility observed in the experiments is due to inertial forces. As a by-product we validate the numerical techniques used—in particular the recently introduced lattice Boltzmann model. [S0031-9007(96)01611-0]

PACS numbers: 47.15.Gf, 02.70.Bf, 02.70.Lq, 47.60.+i

The flow of an incompressible, Newtonian fluid is governed by the nonlinear Navier-Stokes equations, Eqs. (1) and (2), which can be solved exactly only in simple geometries. In flow, which is slow in the sense that the ratio of inertial to viscous forces (the Reynolds number Re) is sufficiently small, the nonlinear inertial term can be neglected to obtain the linear Stokes equation [1]. In contrast to the nonlinear equations, the steady state Stokes equation is invariant under flow reversal and yields exact results in simple geometries, so it has been a matter of fundamental discussion below which value of Re the Stokes approximation to Eq. (2) is justified.

Numerous authors [2–4] have calculated correction factors to the Stokes drag at small, nonzero Reynolds numbers. The corrections are linear in Re and have prefactors of order unity. Correspondingly, streamlines around a cylinder look symmetric in the fore-and-aft direction until Re is of order unity [5]. Generally, for single phase flow the Stokes approximation is considered to be valid if $\mathrm{Re} < 1-5$ [6]. However, when there are finite size particles suspended in the fluid, inertial effects can be observed, in principle, at arbitrary small Reynolds numbers. This is the case in the so-called *tubular pinch* effect, which causes particles suspended in a tube flow to migrate to a stationary off-center position in the tube. The effect, which was first recorded by Poiseuille [7] in blood streams and later studied systematically by Segré and Silberberg [8] cannot be explained without the nonlinear term in the Navier-Stokes equation. But only the transient state, i.e., the speed with which the particles migrate to their steady state position, depends on Re—the final radial position of the particles is Re independent, even in echo experiments [9].

In the present study we observe nonlinear effects at low Re in single phase flow. In contrast to the tubular pinch of suspended particles, the "echo" signal in our single phase experiment with passive tracer molecules depends continuously on Re and thus serves to quantify the role of the nonlinear term, also when its relative magnitude is very small. An immediate conclusion from our measurements is that the proper condition on Re may be highly problem dependent, even in simple flow geometries.

We present echo experiments on creeping flow in a Hele-Shaw channel with an obstacle (see Fig. 1), where a passive tracer is convected forwards and backwards with a carrier fluid such that (ignoring molecular diffusion) each tracer molecule would exactly return to its initial position if the flow were perfectly reversible. Since the flow as described by the Stokes equation is time reversible [10], the echo technique effectively integrates out the reversible part of the velocity field, making the experiment sensitive to any deviation from reversibility.

In the experiments we detect visible departure from reversibility at $\mathrm{Re} \sim 0.02$ through an "M"-shaped deformation of an otherwise perfectly returned tracer line (see Fig. 2), where the size of the deformation increases linearly with increasing Re; see Fig. 3. Comparing the experiments to two independent numerical models—where the deformation is visible already at $\mathrm{Re} \sim 0.0006$—we demonstrate that the observed irreversibility is due to the effect of the nonlinear inertial force, i.e., of hydrodynamic nature.

Experiments.—The experimental setup was previously used to study enhanced dispersion in creeping flow [11,12]. In each experiment, a thin, straight line (radius

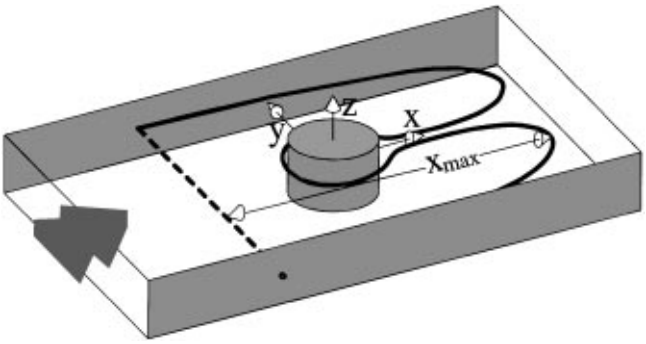

FIG. 1. Sketch of the experiment: During forward convection, a line of passive tracer was convected towards (full line) the cylinder of radius $r = 0.5$ cm in a channel of width 5 cm such that it folded around the cylinder. Upon flow reversal, the tracer line was "echoed" back towards its initial position (dashed line).

 0031-9007/96/77(20)/4170(4)$10.00

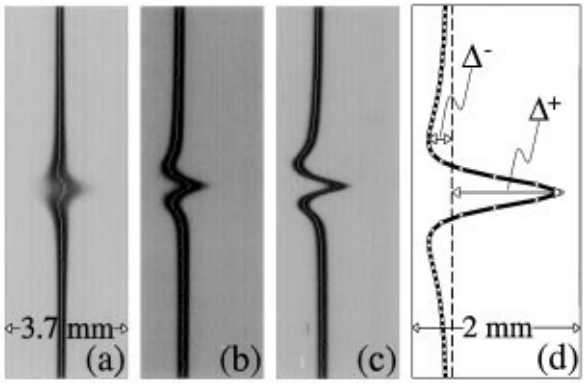

FIG. 2. Enlargements of the characteristic deformation of the returned tracer lines from experiments at Reynolds numbers (a) Re = 0.016, (b) Re = 0.069, and (c) Re = 0.17. White pixels show the calculated coordinates that are used to measure distances. (d) FD simulation at Re ≃ 0.062. Data are compared by measuring Δ^+, Δ^-, and their sum Δ.

$a \simeq 0.3$ mm) of tracer fluid was first placed across the filled cell at a distance of 3 cylinder radii, $r = d/2 = 0.5$ cm, in front of the cylinder center (see Fig. 1). Next, a fixed amount of carrier fluid (glycerol-water mixture) was pumped into the cell at constant volume flux Q. The pump was then abruptly reversed, withdrawing the same amount of fluid. At flow reversal, the maximum extension of the tracer line was approximately $x_{\max} = 10r$, and the smallest distance to the cylinder was $x_{\min} = (0.08 \pm 0.01)r$.

Buoyancy forces on the tracer were minimized by carefully matching the density ($\rho = 1.2318 \pm 0.0001$ g/cm^3) of the two fluids. The viscosity of the carrier fluid was $\mu \simeq 220$ cP, while the viscosity of the tracer was (2–3)% lower. The effect of this viscosity contrast appeared to be negligible. Average flow velocities U between $U = 0.031$ cm/s and $U = 0.28$ cm/s produced Re in the range

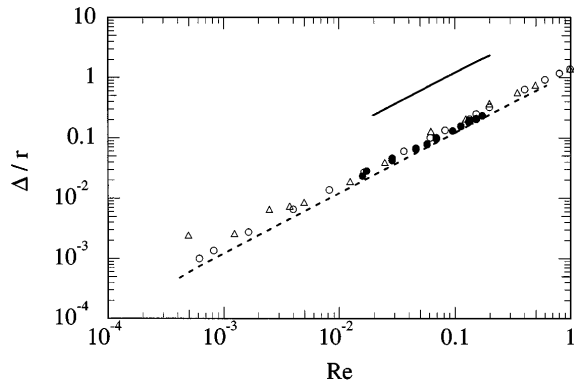

FIG. 3. Peak-to-peak distance Δ of the returned tracer lines as a function of the Reynolds number Re for (●) experiments; (△) lattice Boltzmann simulations; (○) finite difference simulations; (- - -) finite difference simulations of the Oseen equations for experimental geometry; (—) analytic Oseen solution [2] for infinite channel width.

0.016–0.17. The molecular diffusivity of the tracer was $D_m = (2.8 \pm 0.2) \times 10^{-8}$ cm^2/s, giving Péclet numbers Pe $= Ud/D_m$ of the order 10^6–10^7.

Using a photometric CCD camera with a spatial resolution of (20 μm)^2/pixel, we identified the positions $x(y)$ of maximum concentration for all y across the channel (see Fig. 2).

Simulations.—Mathematically the flow is described by the Navier-Stokes equations,

$$\nabla \cdot \boldsymbol{u} = 0\,, \tag{1}$$

$$\rho \frac{\partial \boldsymbol{u}}{\partial t} + \rho \boldsymbol{u} \cdot \nabla \boldsymbol{u} = -\nabla p + \mu \nabla^2 \boldsymbol{u} + \boldsymbol{f}\,. \tag{2}$$

Here $\boldsymbol{u}(\boldsymbol{r}, t)$ denotes the local fluid velocity at position $\boldsymbol{r}$ and time t, p the pressure, and $\boldsymbol{f}$ the external forces [1]. For flow with average velocity U in a geometry with a characteristic length, d, the Reynolds number is Re $= Ud/\nu$, with $\nu = \mu/\rho$.

In the steady state ($\partial \boldsymbol{u}/\partial t = \mathbf{0}$) the reversibility of the flow can be expressed by the invariance of Stokes equation under the transformation $\boldsymbol{u} \rightarrow -\boldsymbol{u}$, $\boldsymbol{f} \rightarrow -\boldsymbol{f}$, and $\nabla p \rightarrow -\nabla p$. This simple symmetry [10] is broken by the presence of the nonlinear term, and, in general, the flow that results from reversal of the external forces must be recomputed. However, in the present case where there is a mirror symmetry of the flow geometry, the reversed flow field is given by $\boldsymbol{u}_r(\boldsymbol{r}) = -\boldsymbol{u}(-\boldsymbol{r})$.

The simulations can be performed in a 2D plane corresponding to the central fluid layer if the modification of the forcing $\boldsymbol{f} \rightarrow \boldsymbol{f} - 8\mu\boldsymbol{u}/h^2$ (where h is the plate separation) is made in Eq. (2) to account for the viscous drag of the top and bottom plates of the cell [12]. This correction factor assumes that the z dependence of $\mathbf{u}$ is parabolic. For the Reynolds number of these quasi 3-D simulations the velocity U must be replaced by $2\bar{U}/3$, where $\bar{U}$ is the average value of $\boldsymbol{u}$ in the central layer.

Steady state solutions to this quasi 3D Navier-Stokes equation were obtained using a lattice Boltzmann (LB) method as well as a finite difference (FD) scheme. To verify the validity of the quasi 3D method, a full 3D FD simulation at Re = 0.01 was computed. The relative difference between the central layer of this 3D field and a quasi 3D calculation of the same average velocity $\bar{U}$ was about 1%.

In the FD scheme a space-discretized version of the steady state Navier-Stokes equation was solved approximately through a relaxation process discussed in Ref. [13] ("artificial compressibility method on a MAC mesh").

The LB method [14] models the fluid as a large number of particles [15] that move from site to site on a triangular lattice, where they interact in mass and momentum conserving collisions. We use the BGK (Bhatnagar, Gross, and Krook) model [16], which differs from other Boltzmann models by a simplified collision operator. The basic variables of the LB models

are the probabilities $N_i(\boldsymbol{r}, t)$ of finding a particle on a site at position $\boldsymbol{r}$ at time t moving with unit velocity in one of the six lattice directions $\boldsymbol{c}_i$, with $i = 1, \ldots, 6$. The precise scheme according to which these probabilities are updated is discussed in Refs. [11,17]. The conserved site densities of mass and momentum are defined as $\rho = \sum_i N_i$ and $\overline{\rho}\boldsymbol{u} = \sum_i \boldsymbol{c}_i N_i$, respectively, where $\overline{\rho}$ is the total averaged density. This definition of $\boldsymbol{u}$ differs from the usual one by the replacement $\rho \rightarrow \overline{\rho}$. This minimizes the slight effects of compressibility [15]. The present application is very sensitive to effects of compressibility and ρ has spatial variations of the order 1%. Provided the Mach number is small the velocity $\boldsymbol{u}$ satisfies the two-dimensional version of Eqs. (1) and (2) with the modification that $\rho\boldsymbol{u} \cdot \nabla\boldsymbol{u} \rightarrow G\rho\boldsymbol{u} \cdot \nabla\boldsymbol{u}$. This extra G factor is a free parameter of the model [11,18]. For steady flows Eqs. (1) and (2) can be recovered by absorbing the factor $1/G$ in ν, P, and $\boldsymbol{f}$. This causes the pertinent Reynolds number to take the (generalized) form $\mathrm{Re} = GUd/\nu$ [12]. For computational efficiency Re was tuned by varying G alone.

Although the FD and LB methods are based on completely different perceptions of the fluid, calculated flow fields were almost identical. The two methods will be compared in detail elsewhere [19]. In both methods, tracer particles were convected by integrating the equation of motion $\dot{\boldsymbol{r}} = \boldsymbol{u}$ with a fourth order Runge Kutta scheme [20], and off-lattice velocities were obtained using linear interpolation schemes.

Results and Discussion.—Qualitatively Fig. 2 shows agreement between LB and FD simulations and experiments. Quantitatively, the main result of this Letter is shown in Fig. 3 where the "peak-to-peak distance," $\Delta = \Delta^+ + \Delta^-$ of the "M"-shaped deformation is plotted as a function of Re for experiments and simulations [see Fig. 2(d)] as well as for the analytic solution of the linear Oseen equation [2] for the flow around a cylinder in the absence of boundary walls. The data give that $\Delta/r = a\,\mathrm{Re}$. For experiments, we find $a_{\mathrm{exp}} = 1.37 \pm 0.03$, while LB and FD simulations lead to the values $a_{lb} \simeq 1.47 \pm 0.1$ and $a_{\mathrm{FD}} \simeq 1.33 \pm 0.03$, respectively. In experiments the M is blurred for $\mathrm{Re} < 0.02$ [see Fig. 2(a)] since enhanced diffusive spreading [11,12] becomes important, and at $\mathrm{Re} \leq 0.004$ this effect dominated. The slope of the Oseen result is larger than the slope of the LB/FD results by almost a factor of 9, thus demonstrating the Oseen solution captures the rough qualitative—but not the quantitative—aspects of the present inertial effects. Solving the Oseen equations for the experimental geometry we find $a_{\mathrm{Os}} = 1.2 \pm 0.03$.

The shape of the M may be understood by inspecting the "difference field" $\boldsymbol{u} + \boldsymbol{u}_r$; see Fig. 4. The net velocity towards the cylinder along the central flow line produces the central kink of the M. It expresses the fact that the flow is slightly slower behind the cylinder. The arches of the M develop through the net transport transverse to the flow since the return streamline is not identical to the forward streamline as illustrated in Fig. 4. This causes the tracer to travel faster during return, making it overreach the starting position. Note, the passive tracers follow the streamlines, and do not move across them.

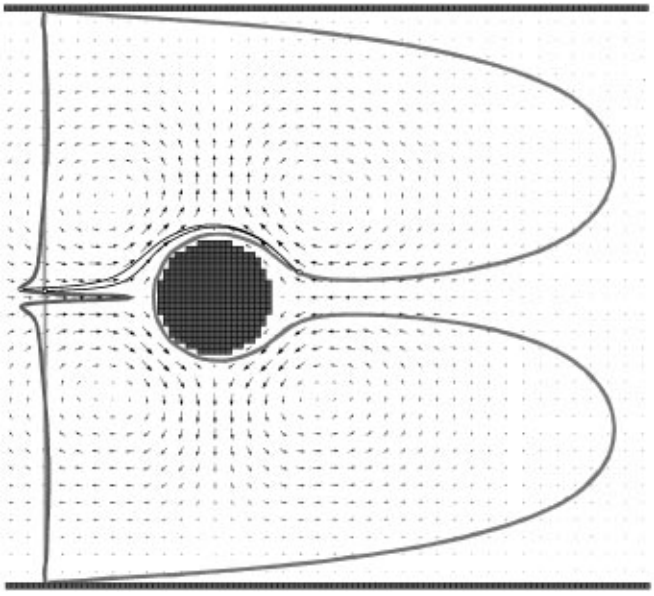

FIG. 4. The *difference* between the forward and reversed velocity field at $\mathrm{Re} = 1.58$. In case of complete reversibility the field should be zero everywhere. The grey lines show the tracer line in the initial straight position, fully stretched at the point of reversal and deformed at the return. The black line represents the path of diffusionless tracer molecules that start on the initial, are convected along with the forward flow and convected back, not retracing its path, to overreach its starting point.

In spite of the good quantitative agreement between experiments and simulations shown in Fig. 3, the exact shape of the returned tracer lines is different in the two cases (see Fig. 2). We find the ratios $\Delta^+/\Delta^- \simeq 1$ and $\simeq 4.7$ for experiments and simulations, respectively. In order to understand this discrepancy a number of simulations were carried out. By varying the channel geometry we found that end effects are insignificant. On the other hand, by including transient effects, modeling the start and reversal of the flow, described by the $\partial\boldsymbol{u}/\partial t$ term in the quasi 3-D version of Eq. (2), we found $\Delta^+/\Delta^- \simeq 3.9$ instead of 4.7. Preliminary investigations indicate that while the ratio Δ^+/Δ^- depends on the time dependent characteristics of the full three dimensional flow field, the sum Δ depends mainly on the nonlinear term [19].

The present problem strongly challenges the numerical methods, since the main signal, the reversible component of the flow field, is integrated out. The agreement between LB and FD simulations and the agreement with experiments therefore provide solid validation of the two numerical models. This is particularly nontrivial for the LB model where the connection with the Navier-Stokes equations is

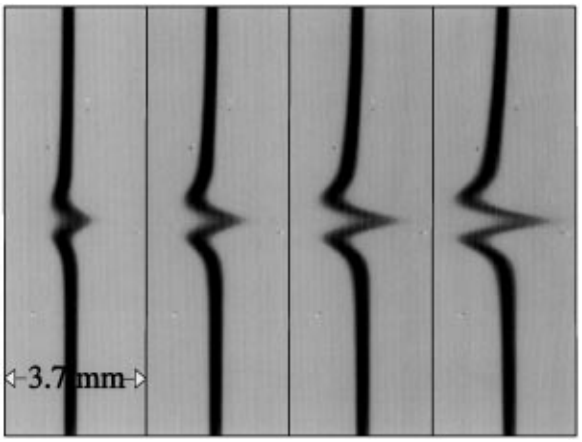

FIG. 5. A tracer line after one, two, three, and four convection cycles at Re = 0.05.

less than obvious [14,15]. However, we have been unable, with our computer resources and algorithms, to obtain the full 3D time dependent solutions to Eqs. (1) and (2), required to get the exact experimental echo profile.

Figure 5 shows an experiment where one tracer line was reversed and returned 4 times. The linear increase of the amplitude Δ with the number of flow reversals can be used as a means to magnify the signal at very small Re. Earlier studies of oscillatory flows [21] have focused on small amplitude oscillations compared to our experiments.

The inherent irreversibility of low Reynolds number flows that we demonstrate is also of interest when discussing experiments on hydrodynamic dispersion where the echo technique is used [11,12,22,23]. Rigord *et al.* [23] performed experiments with a porous medium made of packed glass beads and observed that the spread of the returned tracer profile increased with the Reynolds number, which was in the range $0.2-1.1$ in their case. Our results suggest that some of their observations may be rationalized by considering the effects of the present hydrodynamic, in addition to diffusive, mechanism of irreversibility.

We have discussed a particular case of creeping flow in a Hele-Shaw cell, where inertial effects are experimentally observable for $\mathrm{Re} \geq 0.02$. Numerical simulations of the steady state Navier-Stokes equation reproduced this effect.

The sensitive echo technique could also be used to detect mechanisms other than inertia that destroy reversibility. In particular, it might be used to investigate non-Newtonian behavior of complex fluids like paints, pastes, and polymer solutions. Finally, our results relate to hydrodynamic problems that involve particles in oscillatory flows (see Fig. 5) and to the study of dispersion in porous media.

This work has been supported by NFR (Norwegian Research Council) through Grants No. 100339/431, No. 101874/410, No. 100666/410, and No. 100198/410 and by Grant No. 6311 from VISTA [a research cooperation between the Norwegian Academy of Science and Letters and Den norske stats oljeselskap a.s. (Statoil)], and by Norsk Hydro a.s. T. R. acknowledges a grant of computing time from the Norwegian Super-computing Committee.

[1] L. D. Landau and E. M. Lifshitz, *Fluid Mechanics* (Pergamon Press, New York, 1987), 2nd ed.
[2] H. Lamb, Philos. Mag. **21**, 112 (1911).
[3] I. Proudman and J. R. A. Pearson, J. Fluid Mech. **2**, 237 (1957).
[4] W. Chester and D. Breach, J. Fluid Mech. **37**, 751 (1969).
[5] M. V. Dyke, *An Album of Fluid Motion* (The Parabolic Press, Stanford, CA, 1982).
[6] J. Happel and H. Brenner, *Low Reynolds Number Hydrodynamics* (Prentice Hall Inc., Englewood Cliffs, NJ, 1965).
[7] J. L. M. Poiseuille, Ann. Sci. Nat. **5**, 111 (1836).
[8] G. Segré and A. Silberberg, J. Fluid Mech. **14**, 136 (1962).
[9] L. I. Berge, J. Feder, and T. Jøssang, J. Colloid Interface Sci. **138**, 480 (1990).
[10] F. P. Bretherton, J. Fluid Mech. **14**, 284 (1962).
[11] U. Oxaal, E. G. Flekkøy, and J. Feder, Phys. Rev. Lett. **72**, 3514 (1994).
[12] E. G. Flekkøy, U. Oxaal, J. Feder, and T. Jøssang, Phys. Rev. E **52**, 4952 (1995).
[13] R. Peyret and T. D. Taylor, *Computational Methods for Fluid Flow* (Springer-Verlag, New York, 1983).
[14] G. McNamara and G. Zanetti, Phys. Rev. Lett. **61**, 2332 (1988).
[15] U. Frisch *et al.*, Complex Syst. **1**, 648 (1987).
[16] Y. Qian, D. D'Humières, and P. Lallemand, Europhys. Lett. **17**, 479 (1992).
[17] E. G. Flekkøy, Phys. Rev. E **47**, 4247 (1993).
[18] E. G. Flekkøy, Ph.D. thesis, University of Oslo, 1993.
[19] T. Rage, E. G. Flekkøy, U. Oxaal, and J. Feder (to be published).
[20] W. H. Press, B. P. Flannery, S. A. Teukolsky, and W. T. Vetterling, *Numerical Recipes* (Cambridge University Press, Cambridge, 1986).
[21] E. J. Chang and M. R. Maxey, J. Fluid Mech. **277**, 347 (1994).
[22] J. Hulin and T. J. Plona, Phys. Fluids A **1**, 1341 (1989).
[23] P. Rigord, A. Calvo, and J. Hulin, Phys. Fluids A **2**, 681 (1990).